Journal of Math-for-Industry, Vol. 3 (2011C-5), pp. 33–40

Application of a degenerate diffusion method in medical image processing

Radek Máca, Michal Beneš and Jaroslav Tintěra

Revised on October 25, 2011

Abstract. This paper deals with segmentation of image data using a partial differential equation of level-set type. The first part of this paper describes the level-set formulation and modification of the level-set equation. The evolution process are controlled by the segmented image data in such a way that the edges of objects can be found. The semi-implicit complementary-volume numerical scheme is used for solving the level-set equation. The final part of the paper describes algorithm parameters and their setting used for segmentation of the left heart ventricle in the cardiac MRI images.

Keywords. Cardiac MRI, co-volume method, image segmentation, level set method, PDE

1. Introduction

The presented work is motivated by the need of medical practice for evaluation of the dynamical images of the heart obtained by the magnetic resonance imaging (cardiac MRI). One of the important purposes of cardiac MRI examination is an estimation of parameters reflecting current clinical state of patients. A typical example could be an accurate measurement of heart ventricle volume during the heart contraction showing the contractive ability of myocardium. Within this framework, it is necessary to find the inner contour of the ventricle in the MR images. We attempt to adapt and modify a segmentation model based on numerical solution of a partial differential equation of the level set type. The iterative algorithm is controlled by the segmented image data in such a way that the edges of the objects can be found. The level set equation is solved by the semi-implicit complementary-volume numerical scheme [7], [13], [14]. The prove of stability and consistency of the linear semi-implicit complementary-volume numerical scheme for solving the regularized (in the sense of Evans and Spruck [9]) mean curvature flow equation in the level set formulation can be found in [10]. We describe parameters and their setting used for segmentation of the left heart ventricle from the cardiac MRI images.

A similar model ([1]) used in image segmentation is based on the phase-field approach to the mean curvature flow. The segmentation model is given by the Allen-Cahn equation (see [2]). In [5] and [6] the Allen-Cahn equation is used for segmentation of the left heart ventricle volume and the wall of the left heart ventricle. Over the last years, 3D [7] and 4D (space and time) [3], [12], [13], [15] methods became used in image segmentation. Recently, a priori information carried by the image data has been included into the segmentation models (see [8], [16], [18]).

2. Mathematical model

Our approach is based on level set formulation for the motion of the segmentation curve $\Gamma_t \subset \Omega, \Omega \in \mathbb{R}^2$ propagating in the normal direction with speed V. A detailed description of the level set formulation can be found in [19].

Main idea of the level set method is to describe the motion of $\Gamma(t)$ by means of the zero level set of a function $u : [0,T] \times \Omega \to \mathbb{R}$ such that

$$\Gamma(t) = \{x \in \Omega \,|\, u(t,x) = 0\}\,. \tag{1}$$

We define the signed distance function (SDF) needed for our approach:

Definition 2.1. Let Γ be a closed curve in $\Omega \subset \mathbb{R}^2$ for which $\Gamma_{\text{in}} = \operatorname{int}\Gamma$, $\Gamma_{\text{out}} = \operatorname{ext}\Gamma$ are defined and satisfies $\Gamma = \partial\Gamma_{\text{in}} = \partial\Gamma_{\text{out}}$, $\Gamma_{\text{in}} \cup \Gamma \cup \Gamma_{\text{out}} = \Omega$. We define the signed distance function (d_Γ) as

$$d_\Gamma(x) = \begin{cases} \operatorname{dist}(x,\Gamma) & x \in \Gamma_{\text{out}}\,, \\ 0 & x \in \Gamma\,, \\ -\operatorname{dist}(x,\Gamma) & x \in \Gamma_{\text{in}}\,, \end{cases}$$

where $\operatorname{dist}(x,\Gamma) = \min\{|x-y| \,|\, y \in \Gamma\}\,.$

For a given initial closed simple curve Γ_0, we can define u_{ini} as follows

$$u_{\text{ini}}(x) = u(0,x) = d_{\Gamma_0}(x) \qquad \forall x \in \Omega\,. \tag{2}$$

Using level set formulation we can derive following evolution equation which implicitly describes the motion of $\Gamma(t)$ given by (1) with speed V in the outward normal direction.

$$\frac{\partial u}{\partial t} + V|\nabla u| = 0\,. \tag{3}$$

The function $u(t,x)$ will be referred to as the segmentation function. For certain form of the speed function V one

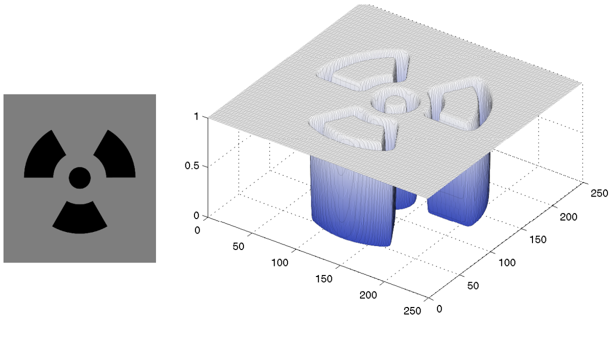

(a) (b)

Figure 1: The testing image (a) and the corresponding edge detector (b).

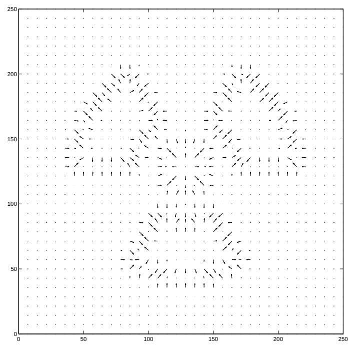

Figure 2: The velocity field of the advection term for the image in Fig. 1a.

obtains a standard Hamilton-Jacobi equation. Specifically, we consider the following form of the normal velocity

$$V = -\kappa + F = -\nabla \cdot \frac{\nabla u}{|\nabla u|} + F\,, \tag{4}$$

where κ is the mean curvature of each level set defined as the divergence of its normal vector and F is an external force term. Substituting (4) to equation (3), we obtain the level set equation in the form

$$u_t = |\nabla u|\, \nabla \cdot \frac{\nabla u}{|\nabla u|} - |\nabla u|\, F\,, \tag{5}$$

where we denote $u_t := \partial u/\partial t$. Modification of the level set equation in the form

$$u_t = |\nabla u|_\varepsilon \nabla \cdot \frac{\nabla u}{|\nabla u|_\varepsilon} - |\nabla u|_\varepsilon F\,, \tag{6}$$

where $|\nabla u| \approx |\nabla u|_\varepsilon = \sqrt{\varepsilon^2 + |\nabla u|^2}$ denotes a regularization, can be used as a tool to prove existence of viscosity solution of the level set equation (see [9]). In this work ε is a computational parameter; its value is set to $\varepsilon = 0.001$.

Detection of image object edges (boundaries) is a known task in image segmentation. Edges in the input image (denoted by I^0 and represented by the matrix $n_{x_1} \times n_{x_2}$ with values $0, 1, \ldots, I_{\max}$) can be recognized by the magnitude of its spatial gradient. Application of the level set equation in this area requires an adaptation as follows

$$\begin{aligned} u_t =& |\nabla u|_\varepsilon \nabla \cdot \left(g\left(\left|I^0 * \nabla G_\sigma\right|\right) \frac{\nabla u}{|\nabla u|_\varepsilon} \right) \\ &- g\left(\left|I^0 * \nabla G_\sigma\right|\right) |\nabla u|_\varepsilon F\,, \end{aligned} \tag{7}$$

where $g : \mathbb{R}_0^+ \to \mathbb{R}^+$ is a non-increasing function for which $g(0) = 1$ and $g(s) \to 0$ for $s \to +\infty$. This function was first used by P. Perona and J. Malik ([17]) to modify a heat equation into a nonlinear diffusion equation which maintains edges in an image. Consequently, the function g is called the Perona-Malik function. We put $g(s) = 1/(1 + \lambda s^2)$ with $s \geq 0$. $G_\sigma \in \mathcal{C}^\infty(\mathbb{R}^2)$ is a smoothing kernel, e.g. the Gauss function with zero mean and variance σ^2

$$G_\sigma(x) = \frac{1}{\sqrt{2\pi\sigma^2}} e^{-\frac{|x|^2}{2\sigma^2}}\,,$$

which is used for pre-smoothing (denoising) of image gradients by convolution

$$(I^0 * \nabla G_\sigma)(x) = \int_{\mathbb{R}^2} \bar{I}^0(x - y) \nabla G_\sigma(y)\, \mathrm{d}y\,,$$

where $\bar{I}^0$ is the extension of I^0 to $\mathbb{R}^2$ by, e.g. mirroring, periodic prolongation or zero padding. Let us note that equation (7) can be rewritten into the advection-diffusion form

$$u_t = \underbrace{g^0 |\nabla u|_\varepsilon \nabla \cdot \left(\frac{\nabla u}{|\nabla u|_\varepsilon} \right)}_{(D)} + \underbrace{\nabla g^0 \cdot \nabla u}_{(A)} - \underbrace{g^0 |\nabla u|_\varepsilon F}_{(F)}\,. \tag{8}$$

For convenience, we use the abbreviation $g^0 = g(\left|I^0 * \nabla G_\sigma\right|)$. (D) in (8) denotes the diffusion term, (A) the advection term and (F) the external force term. The term g^0 is called the edge detector. For an example of an edge detector, see Fig. 1b. We can observe that value of the edge detector is approximately equal to zero close to image edges. Here the evolution of the segmentation function slows down. On the contrary, the edge detector equals one in parts of the image with constant intensity. As we can see in Figure 2, the advection term attracts the segmentation function to the image edges. We propose an advection parameter $\mathcal{A}$ to change the magnitude of the advection term. Obviously, in an image might be parts where $\partial g^0 = 0$ and there the advection term does not contribute to the evolution of the function u and the zero level set as well. Using the SDF as an initial condition the external force term becomes an essential part of the segmentation model. Finally, we obtain the final form of the modified level set equation, namely

$$u_t = g^0 |\nabla u|_\varepsilon \nabla \cdot \left(\frac{\nabla u}{|\nabla u|_\varepsilon} \right) + \mathcal{A} \nabla g^0 \cdot \nabla u - g^0 |\nabla u|_\varepsilon F\,. \tag{9}$$

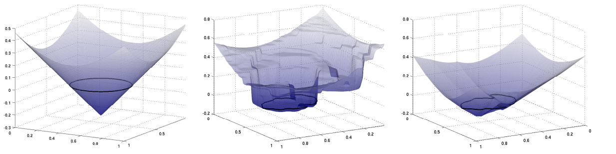

Figure 3: Example of segmentation function. Initial segmentation function u_0 (left), segmentation function u for $(t > 0)$ (middle), restored SDF (right).

2.1. Initial condition

A segmentation function $u(t, x)$ evolves from the initial guess (2). The initial curve Γ_0 has to be placed inside the segmented area (inside the left heart ventricle). To expand the initial curve, velocity (4) has to be positive. Positive value of V implies positive value of the external force F, rather $F > \kappa$. In other words, the zero level set is forced to expand in regions where the advection term does not contribute to the evolution of the function u. We use the signed distance function (SDF) for setting and restoring (redistancing) of the initial condition.

At the beginning of segmentation, i.e. for the first image, we have to place the initial curve Γ_0 into the left heart ventricle manually, e.g. as a circle. For a given Γ_0 we construct SDF d_{Γ_0} and set the initial condition as $u_{\text{ini}} = d_{\Gamma_0}$. The segmentation function u evolves from the initial guess (Fig. 3 left) according to (7). This evolution distorts the original shape of u_{ini} into $u(t, x)$ which fails to have unit gradient slopes (Fig. 3 middle). At the beginning of next image segmentation it is convenient to use the result of previous image segmentation $\Gamma_t = \{x \in \mathbb{R}^2 \,|\, u(t, x) = 0\}$ and its signed distance function d_{Γ_t} as a new initial condition.

This is performed by means of the fast sweeping method introduced in [20]. This method is used for computing the viscosity solution of the eikonal equation

$$\begin{aligned} |\nabla u(x)| &= 1 \qquad && x \in \Omega\,, \\ u(x) &= 0 && x \in \Gamma \subset \Omega\,. \end{aligned}$$

Example of the restored signed distance function is shown in Figure 3 on the right.

3. Numerical scheme

A semi-implicit co-volume space discretization is used for solving (9) numerically. In [7], [10], [11], [14] a semi-implicit co-volume method discretizing (7) without the external force term is presented. First, we choose a uniform discrete time step τ. Then we replace time derivative in (9) by backward difference. The linear terms of the equation are considered at the current time level while the nonlinear terms (i.e. $|\nabla u|_\varepsilon$) are treated from the previous time level. In this way we obtain the following semi-implicit

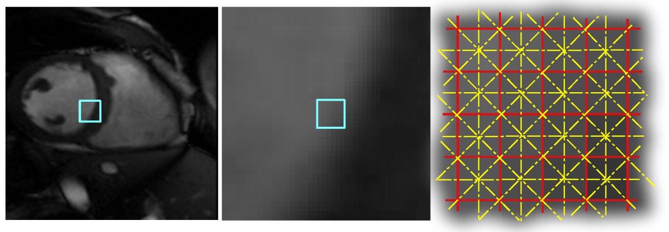

Figure 4: Input image (left), first zoom of input image (middle) and second zoom (right) with triangulation (dashed lines) and image structure corresponding to co-volume mesh (solid lines).

discretization

$$\begin{aligned} \frac{u^k - u^{k-1}}{\tau} =& g^0 |\nabla u^{k-1}|_\varepsilon \nabla \cdot \left(\frac{\nabla u^k}{|\nabla u^{k-1}|_\varepsilon} \right) \\ & + \mathcal{A} \nabla g^0 \cdot \nabla u^k - g^0 |\nabla u^{k-1}|_\varepsilon F\,. \end{aligned} \tag{10}$$

To simplify construction of spatial discretization, we rewrite the previous equation using the following expression

$$g^0 \nabla \cdot \left(\frac{\nabla u^k}{|\nabla u^{k-1}|_\varepsilon} \right) = \nabla \cdot \left(g^0 \frac{\nabla u^k}{|\nabla u^{k-1}|_\varepsilon} \right) - \nabla g^0 \cdot \frac{\nabla u^k}{|\nabla u^{k-1}|_\varepsilon}\,. \tag{11}$$

Now we substitute (11) to (10). Dividing by $|\nabla u^{k-1}|_\varepsilon$, we get new form of (10)

$$\begin{aligned} \frac{1}{|\nabla u^{k-1}|_\varepsilon} \frac{u^k - u^{k-1}}{\tau} =& \nabla \cdot \left(g^0 \frac{\nabla u^k}{|\nabla u^{k-1}|_\varepsilon} \right) \\ & + (\mathcal{A} - 1) \frac{1}{|\nabla u^{k-1}|_\varepsilon} \nabla g^0 \cdot \nabla u^k - g^0 F\,. \end{aligned} \tag{12}$$

To construct a fully-discrete system of equations, we use the co-volume method. The digital image is recorded on a structure of pixels with rectangular shape. Each pixel includes values of I^0 influencing the segmentation model. We relate spatial approximations of the segmentation function u to the centers of image pixels. We evaluate the gradients of the segmentation function at the previous time step ($|\nabla u^{k-1}|_\varepsilon$) in (12). We put a triangulation inside the pixel structure and use a piecewise linear approximation of the segmentation function on this triangulation. This approach gives constant value of gradient on each triangle. For a given pixel structure we build a triangulation in such a way that the centers of pixels are connected by new rectangular mesh. Each new rectangle is divided into four triangles of equal size (see Fig. 4). The pixel centers will be called degree-of-freedom (DF) nodes. Other nodes (at intersection of solid lines in Figure 4) will be called non-degree-of-freedom (NDF) nodes. Let a function u be given by discrete values at DF nodes and u_h be a piecewise linear approximation of u on the triangulation. The value u_h at NDF nodes is given by average value of the neighboring DF nodal values.

For triangulation $\mathcal{T}_h$ given by the previous construction, we construct a co-volume (dual) mesh consisting of cells p associated with DF nodes p of $\mathcal{T}_h$ only. Without any confusion, we denote each co-volume and the corresponding DF node by the same symbol. In order to derive the co-volume spatial discretization let us introduce the notation in Table 1.

C_p	...	set of all DF nodes q connected to the node p by an edge
σ_{pq}	...	edge connecting DF nodes p and q
h_{pq}	...	length of σ_{pq}
e_{pq}	...	common edge of co-volumes p and q ($\partial p = \bigcup_{q\in C_p} e_{pq}$)
$\mathcal{E}_{pq}$	...	set of triangles including the edge σ_{pq}
c_{pq}^T	...	length of the portion of e_{pq} that is in $T \in \mathcal{T}_h$ ($c_{pq}^T = \lvert e_{pq}^T \cap T\rvert$)
$\mathcal{N}_p$	...	set of $T \in \mathcal{T}_h$ including the vertex p
$\lvert\nabla u_T\rvert$	...	value of $\lvert\nabla u_h\rvert$ on $T \in \mathcal{T}_h$
u_p	...	value of $u_h(x_p)$, where x_p is the coordinate of the node p on $\mathcal{T}_h$
u_{pq}	...	value of $u_h(x_{\frac{pq}{2}})$, where $x_{\frac{pq}{2}} = \sigma_{pq} \cap e_{pq}$
ν_p	...	outer normal of co-volume p
ν_{pq}	...	outer normal of co-volume p on e_{pq}

Table 1: Co-volume notations.

We integrate (12) over each co-volume p, $p \in 1,\dots,M$ (M denotes the number of all DF nodes). The approximation of the left-hand side and the first term on the right-hand side of (12) can be found in [14]. Hence we provide a result of approximation of these two terms without explanation. The left-hand side of (12) is approximated by

$$\int_p \frac{1}{|\nabla u^{k-1}|_\varepsilon}\frac{u^k-u^{k-1}}{\tau}\,\mathrm{d}x \approx m(p)M_p^{k-1}\frac{u_p^k-u_p^{k-1}}{\tau}\,, \tag{13}$$

where $m(p)$ is the measure of co-volume p in $\mathbb{R}^2$ and M_p^{k-1} is given by

$$M_p^{k-1} = \frac{1}{|\nabla u_p^{k-1}|_\varepsilon}\,,\quad |\nabla u_p^{k-1}| = \sum_{T\in\mathcal{N}_p}\frac{m(T\cap p)}{m(p)}|\nabla u_T^{k-1}|\,,$$

where $T\cap p$ is the intersection of triangle T and co-volume p. In our case for $T \in \mathcal{N}_p$, it holds $m(T\cap p)/m(p) = 1/8$. Denoting the spatial step of the co-volume mesh by h, we get $m(p) = h^2$. The approximation of the first term on the right-hand side of (12) is in the form

$$\int_p \nabla\cdot\left(g^0\frac{\nabla u^k}{|\nabla u^{k-1}|_\varepsilon}\right)\mathrm{d}x \approx \sum_{q\in C_p}\left(\sum_{T\in\mathcal{E}_{pq}} c_{pq}^T\frac{g_T^0}{|\nabla u_T^{k-1}|_\varepsilon}\right)\frac{u_q^k-u_p^k}{h_{pq}}\,, \tag{14}$$

where g_T^0 denotes approximation of g^0 on a triangle $T \in \mathcal{T}_h$. The advection term on the right-hand side of (12) is approximated by the first-order upwind scheme. We use the following approximation

$$\int_p (\mathcal{A}-1)\frac{1}{|\nabla u^{k-1}|_\varepsilon}\nabla g^0\cdot\nabla u^k\,\mathrm{d}x \approx (\mathcal{A}-1)M_p^{k-1}\int_p \nabla g^0\cdot\nabla u^k\,\mathrm{d}x\,.$$

Now we rewrite the scalar product of ∇g^0 and ∇u^k into the form

$$\nabla g^0\cdot\nabla u^k = \nabla\cdot\left(\nabla g^0 u^k\right) - \Delta g^0 u^k\,.$$

Then we get

$$\int_p \nabla g^0\cdot\nabla u^k\,\mathrm{d}x = \int_p \nabla\cdot\left(\nabla g^0 u^k\right)\,\mathrm{d}x - \int_p \Delta g^0 u^k\,\mathrm{d}x\,. \tag{15}$$

The first term on the right hand side of (15) is approximated as follows

$$\int_p \nabla\cdot\left(\nabla g^0 u^k\right)\,\mathrm{d}x = \int_{\partial p}\frac{\partial g^0}{\partial\nu_p}u^k\,\mathrm{d}s \approx \sum_{q\in C_p}|e_{pq}|\frac{\partial g^0}{\partial\nu_{pq}}u_{pq}^k\,. \tag{16}$$

For the second term on the right hand side of (15) the divergence theorem implies

$$\int_p \Delta g^0 u^k\,\mathrm{d}x \approx u_p^k\int_p \Delta g^0\,\mathrm{d}x = u_p^k\int_{\partial p}\frac{\partial g^0}{\partial\nu_p}\,\mathrm{d}s \approx u_p^k\sum_{q\in C_p}\int_{e_{pq}}\frac{\partial g^0}{\partial\nu_{pq}}\,\mathrm{d}s \approx u_p^k\sum_{q\in C_p}|e_{pq}|\frac{\partial g^0}{\partial\nu_{pq}}\,. \tag{17}$$

Now we can substitute (16) and (17) into (15) to get

$$\int_p \nabla g^0\cdot\nabla u^k\,\mathrm{d}x \approx \sum_{q\in C_p}|e_{pq}|\frac{\partial g^0}{\partial\nu_{pq}}\left(u_{pq}^k - u_p^k\right)\,.$$

To complete approximation of the advection term we need to evaluate u_{pq}^k. As mentioned above, we use the first-order upwind scheme

$$u_{pq}^k := \begin{cases} u_p^k & \text{for } \frac{\partial g^0}{\partial\nu_{pq}} > 0 \\ u_q^k & \text{for } \frac{\partial g^0}{\partial\nu_{pq}} < 0 \end{cases}\,.$$

Finally the above expressions are put together to get spatial approximation of the advection term

$$\int_p (A-1)\frac{1}{|\nabla u^{k-1}|_\varepsilon}\nabla g^0\cdot\nabla u^k\,\mathrm{d}x \approx (\mathcal{A}-1)M_p^{k-1}\sum_{q\in C_p}|e_{pq}|\min\left(\frac{\partial g^0}{\partial\nu_{pq}},0\right)\left(u_q^k-u_p^k\right)\,. \tag{18}$$

The force term on the right-hand side of (15) is approximated as follows

$$\int_p g^0 F\,\mathrm{d}x \approx m(p)g_p^0 F\,, \tag{19}$$

where g^0_p denotes approximation of g^0 on the co-volume p. Using the notation

$$\begin{aligned} a^{k-1}_{pq} =& \frac{1}{h_{pq}} \sum_{T \in \mathcal{E}_{pq}} c^T_{pq} \frac{g^0_T}{|\nabla u^{k-1}_T|_\varepsilon} \,, \\ g_{pq} =& |e_{pq}| \min\left(\frac{\partial g^0}{\partial \nu_{pq}}, 0 \right) \,, \end{aligned} \tag{20}$$

together with (13), (14), (18) and (19), gives the fully-discrete semi-implicit co-volume scheme

$$\begin{aligned} \Big[m(p) M^{k-1}_p + \tau \textstyle\sum_{q \in C_p} \left(a^{k-1}_{pq} + (\mathcal{A}-1) M^{k-1}_p g_{pq} \right) \Big] u^k_p \\ - \tau \textstyle\sum_{q \in C_p} \left(a^{k-1}_{pq} + (\mathcal{A}-1) M^{k-1}_p g_{pq} \right) u^k_q \\ = m(p) M^{k-1}_p u^{k-1}_q - m(p) g^0_p F \,. \end{aligned} \tag{21}$$

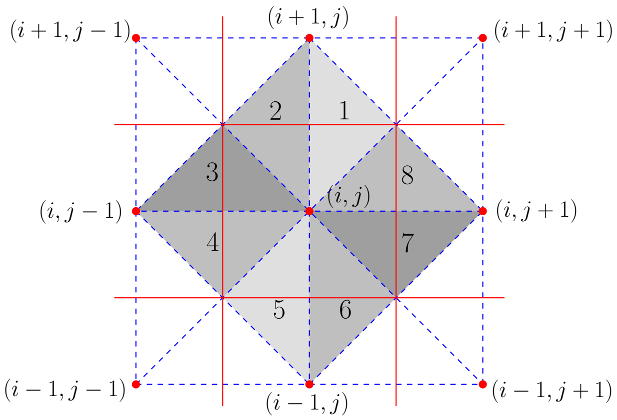

Figure 5: Co-volume p associated with a couple (i,j) and set of 8 triangles $\mathcal{N}_{i,j}$ denoted by numbers 1 to 8.

For simplicity of implementation we can write the co-volume scheme in the "finite-difference notation". Let I^0 be the input image whose size is $n_{x_1} \times n_{x_2}$ where n_{x_1} represents number of pixels in the horizontal direction and n_{x_2} in the vertical direction. We associate the co-volume p and its corresponding DF node with a couple (i,j), where $i \in \{1,\dots,n_{x_2}\}$, $j \in \{1,\dots,n_{x_1}\}$. Using this notation, the unknown value u^k_p is associated with $u^k_{i,j}$ and $\mathcal{N}_p$ with $\mathcal{N}_{i,j}$. As we can see from the coefficient (20), we need to compute absolute value of the gradient on each triangle from the set $\mathcal{N}_{i,j}$ (see Fig. 5) denoted by $G^n_{i,j}$, $n \in \{1,\dots,8\}$ at each discrete time step $k \in \{1,\dots,s\}$ and for every $i \in \{2,\dots,n_{x_2}-1\}$, $j \in \{2,\dots,n_{x_1}-1\}$ (except boundary pixels). For this purpose we use the following expression using discrete values of u^{k-1}, i.e. the value of u from the previous time step. For example $\left|G^1_{i,j}\right|^2$ is in the form

$$\begin{aligned} |G^1_{i,j}|^2 = \left(\frac{u^{k-1}_{i,j+1} + u^{k-1}_{i+1,j+1} - u^{k-1}_{i,j} - u^{k-1}_{i+1,j}}{2h} \right)^2 \\ + \left(\frac{u^{k-1}_{i+1,j} - u^{k-1}_{i,j}}{h} \right)^2 \,. \end{aligned} \tag{22}$$

Other gradient discretization $G^2_{i,j}, \dots, G^8_{i,j}$ can be found in [14]. In the same way (but in the beginning of the algorithm only) we compute values $G^{\sigma,n}_{i,j}, n \in 1,\dots,8$ replacing u^{k-1} by $I^{0,\sigma} := I^0 * G_\sigma$ in the previous expressions (22), e.g.

$$\begin{aligned} \left| G^{\sigma,1}_{i,j} \right|^2 = \left(\frac{I^{0,\sigma}_{i,j+1} + I^{0,\sigma}_{i+1,j+1} - I^{0,\sigma}_{i,j} - I^{0,\sigma}_{i+1,j}}{2h} \right)^2 \\ + \left(\frac{I^{0,\sigma}_{i+1,j} - I^{0,\sigma}_{i,j}}{h} \right)^2 \,. \end{aligned}$$

The convolution $I^0 * G_\sigma$ can be evaluated numerically as the solution of the linear heat equation at the time $t = \sigma^2/2$ with initial condition given by I^0. For each $i \in \{2,\dots,n_{x_2}-1\}$, $j \in \{2,\dots,n_{x_1}-1\}$ we construct north, west, south and east coefficients

$$\begin{aligned} n_{ij} &= \tau \tfrac{1}{2} \textstyle\sum_{n=1}^{2} \frac{g(G^{\sigma,n}_{i,j})}{\sqrt{\varepsilon^2 + (G^n_{i,j})^2}} \\ &\quad + \tau h (\mathcal{A}-1) m_{i,j} \min\left(\frac{g(G^\sigma_{i+1,j}) - g(G^\sigma_{i,j})}{h}, 0 \right) \,, \\ w_{ij} &= \tau \tfrac{1}{2} \textstyle\sum_{n=3}^{4} \frac{g(G^{\sigma,n}_{i,j})}{\sqrt{\varepsilon^2 + (G^n_{i,j})^2}} \\ &\quad + \tau h (\mathcal{A}-1) m_{i,j} \min\left(\frac{g(G^\sigma_{i,j-1}) - g(G^\sigma_{i,j})}{h}, 0 \right) \,, \\ s_{ij} &= \tau \tfrac{1}{2} \textstyle\sum_{n=5}^{6} \frac{g(G^{\sigma,n}_{i,j})}{\sqrt{\varepsilon^2 + (G^n_{i,j})^2}} \\ &\quad + \tau h (\mathcal{A}-1) m_{i,j} \min\left(\frac{g(G^\sigma_{i-1,j}) - g(G^\sigma_{i,j})}{h}, 0 \right) \,, \\ e_{ij} &= \tau \tfrac{1}{2} \textstyle\sum_{n=7}^{8} \frac{g(G^{\sigma,n}_{i,j})}{\sqrt{\varepsilon^2 + (G^n_{i,j})^2}} \\ &\quad + \tau h (\mathcal{A}-1) m_{i,j} \min\left(\frac{g(G^\sigma_{i,j+1}) - g(G^\sigma_{i,j})}{h}, 0 \right) \,, \end{aligned}$$

where $m_{i,j}$ denotes the following expression

$$m_{i,j} = \frac{1}{\sqrt{\varepsilon^2 + \left(\frac{1}{8} \sum_{n=1}^{8} G^{\sigma,n}_{i,j} \right)^2}} \,.$$

If we define diagonal coefficients by

$$c_{i,j} = n_{i,j} + w_{i,j} + s_{i,j} + e_{i,j} + m_{i,j} h^2$$

and right hand sides at the kth discrete time step by

$$r_{ij} = m_{i,j} h^2 u^{k-1}_{i,j} - \tau h^2 G^\sigma_{i,j} F \,,$$

then for the couple (i,j) we get

$$c_{i,j} u^k_{i,j} - n_{i,j} u^k_{i+1,j} - w_{i,j} u^k_{i,j-1} - s_{i,j} u^k_{i-1,j} - e_{i,j} u^k_{i,j+1} = r_{i,j} \,. \tag{23}$$

Collecting these equations for inner DF nodes with the Neumann boundary condition we get a linear system to be solved. We solve this system by the SOR (Successive Over-Relaxation) iterative method.

4. Results

In this section we present the results obtained by our algorithm using the linear system (23) with the Neumann boundary condition. To apply this scheme we have to specify correct values of the parameters of equation (9). The

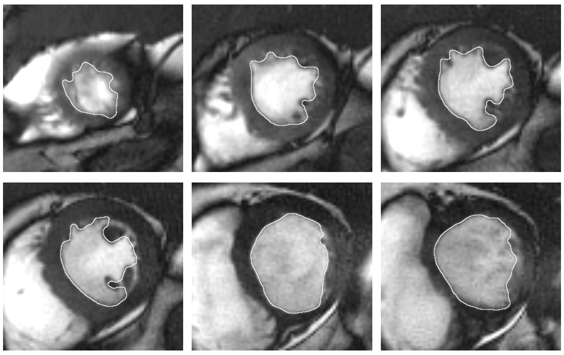

(a) Result of segmentation (end-diastole).

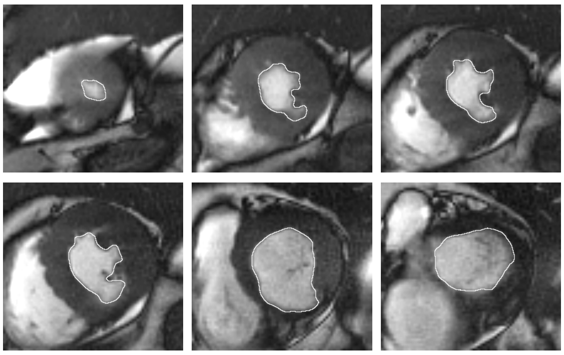

(b) Result of segmentation (end-systole).

Figure 6: Segmentation result for (a) end-diastole and (b) end-systole with parameters $h = 0.0034$, $\lambda = 0.25$, $\mathcal{A}_{\text{out}} = 2$, $F_{\text{out}} = -10$, $F_{\text{in}} = 50$.

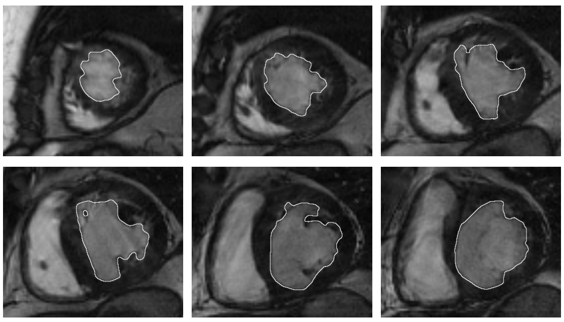

(a) Result of segmentation (end-diastole).

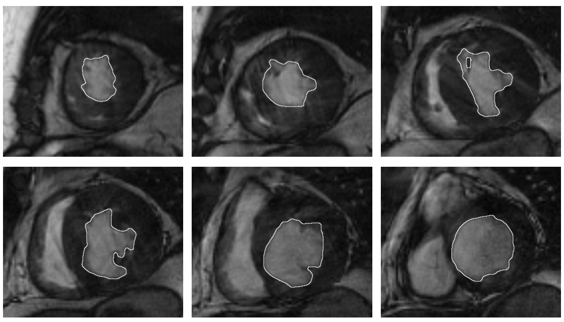

(b) Result of segmentation (end-systole).

Figure 7: Segmentation result for (a) end-diastole and (b) end-systole with parameters $h = 0.0028$, $\lambda = 0.25$, $\mathcal{A}_{\text{out}} = 2$, $F_{\text{out}} = -10$, $F_{\text{in}} = 50$.

sensitivity of the edge detector depends on value of the parameter λ. Very low values of λ decrease the efficiency of edge detection. On the other hand, very high values of λ can cause detection of spurious edges (i.e. noise, blood flow artifacts, etc.). In our work we set $\lambda = 0.25$. We propose an image dependent setting of the force parameter F and of the advection parameter $\mathcal{A}$. In the cardiac MR images obtained by means of the bright blood technique (see [4], chapter 4), the blood in the ventricle is lighter than the myocardium and the surrounding tissue. Also, blood in the ventricles has higher intensity than the myocardium. Using this information we can set a threshold I_{in} for picture elements certainly inside the ventricle and a threshold I_{out} for picture elements certainly in the myocardium and the surrounding tissue. These thresholds are set automatically using an algorithm based on minimum search on selected image slices for a given initial condition. We then propose external force parameter in the form

$$F(I^0) = \begin{cases} F_{\text{out}} & I^0 \leq I_{\text{out}}\,, \\ F_{\text{in}} \left(\frac{I^0 - I_{\text{out}}}{I_{\text{in}} - I_{\text{out}}} \right) & I_{\text{out}} < I^0 < I_{\text{in}}\,, \\ F_{\text{in}} & I^0 \geq I_{\text{in}}\,, \end{cases} \tag{24}$$

where F_{out} is the value of the force parameter for the picture elements certainly outside the left ventricle and F_{in} is the value of the force parameter for the picture elements certainly inside the left ventricle. For the picture elements certainly outside the ventricle we need to shrink the evolution curve. Then the value of F_{out} has to be negative. The value F_{in} has to be positive, as we discussed in Section 2.1. Similarly we propose the advection term, namely

$$\mathcal{A}(I^0) = \begin{cases} \mathcal{A}_{\text{out}} & I^0 \leq I_{\text{out}}\,, \\ (\mathcal{A}_{\text{out}} - 1) \left(1 - \frac{I^0 - I_{\text{out}}}{I_{\text{in}} - I_{\text{out}}} \right) + 1 & I_{\text{out}} < I^0 < I_{\text{in}}\,, \\ 1 & I^0 \geq I_{\text{in}}\,, \end{cases} \tag{25}$$

where $\mathcal{A}_{\text{out}} > 1$. This means that edges with lower intensity are more important than edges with higher intensity. The spatial discrete step is denoted by h and is given as $h = 1/(\max\{n_{x_1}, n_{x_2}\} - 1)$, the temporal discrete time step τ is given by $\tau = h/5$ and σ is set to the value $\sigma = 3h$.

In our work we dealt with non-constant choice of parameters F (24) and $\mathcal{A}$ (25), which is fundamental to obtain good segmentation results. The strong dependence of the algorithm on the thresholds I_{in} and I_{out} could be considered a hindrance. Wrong settings of these thresholds can cause incorrect segmentation results. Therefore it is important to apply robust automatic threshold selection. The results of segmentation can be seen in Fig. 6 and 7. The images are depicted in the end-diastolic phase (maximal volume of the ventricle) and in the end-systolic phase (minimum volume of the ventricle).

5. Conclusion

In the presented paper we adapted the segmentation model based on the level set formulation to the problem of cardiac MRI data segmentation. For the modified level-set equation we introduced a numerical scheme using the semi-implicit discretization in time and the co-volume method for spatial discretization. We proposed new advection and force parameter which depend on input image intensities. Our algorithm is applied to real cardiac MRI data[1].

Acknowledgments

This work was supported by the grant of the Ministry of Education of the Czech Republic MSM6840770010 "Applied Mathematics in Technical and Physical Sciences", by the project "Jindřich Nečas Center for Mathematical Modeling", No. LC06052 of the Ministry of Education of the Czech Republic and by the project "Advanced Supercomputing Methods for Implementation of Mathematical Models" of the Student Grant Agency of the Czech Technical University in Prague No. SGS11/161/OHK4/3T/14.

References

[1] Beneš, M.: Phase field model of microstructure growth in solidification of pure substances, *PhD thesis, Faculty of Nuclear Sciences and Physical Engineering, Czech Technical University in Prague*, (1997)

[2] Beneš, M., Chalupecký, V., Mikula, K.: Geometrical image segmentation by the Allen-Cahn equation, *Applied Numerical Mathematics 51* (2004). 187–205

[3] Besbes, A., Komodakis, N., Glocker, B., Tziritas, G., Paragios N.: 4D Ventricular Segmentation and Wall Motion Estimation Using Efficient Discrete Optimization, *3rd International Symposium in Visual Computing (ISVC'07)*

[4] Bogaert, J., Dymarkowski, S., Taylor, A. M.: Clinical cardiac MRI, *Springer-Verlag*, Berlin Heidelberg, (2005)

[5] Chabiniok, R.: Cardiac MRI Data Segmentation Using the Partial Differential Equation of Allen–Cahn Type, *Master thesis, Faculty of Mathematics and Physics, Charles University in Prague* (2007)

[6] Chabiniok, R., and Tintěra, J.: Cardiac MRI data segmentation using the partial differential equation of Allen–Cahn type, *Beneš M., Kimura M. and Nakaki T., Eds. Proceedings of Czech Japanese Seminar in Applied Mathematics 2006, in COE Lecture Note, Vol. 6, Faculty of Mathematics, Kyushu University Fukuoka, ISSN 1881-4042,* (2007), 37–49

[7] Corsaro, S., Mikula, K., Sarti, A., Sgallari, F.: Semi-implicit co-volume method in 3D image segmentation, *SIAM Journal on Scientific Computing, Vol. 28*, No. 6 (2006), 2248–2265

[8] Crandall, M. G., Ishii, H., Lions, P.-L.: User's guide to viscosity solutions of second-order partial differential equations, *Bul. AMS* **27** (1992), 1–67

[9] Evans, L. C., and Spruck, J.: Motion of level sets by mean curvature I, *J. Diff. Geom., Vol. 33*, (1991), 381–635

[10] Handlovičová, A., Mikula, K.: Stability and consistency of the semi-implicit co-volume scheme for regularized mean curvature flow equation in level set formulation, *Applications of Mathematics*, Vol. 53, No. 2 (2008), 105–129

[11] Handlovičová, A., Mikula, K., Sarti, A.: Numerical solution of parabolic equations related to level set formulation of mean curvature flow, *Computing and Visualization in Science , Vol.1, No. 3*, (1998), 179–182

[12] Lynch, M., Ghita, O., Whelan, P. F.: Segmentation of the Left Ventricle of the Heart in 3D+t MRI Data Using an Optimized Non-Rigid Temporal Model, *IEEE Transactions on Medical Imaging 27(2)*, (2008), 195–203

[13] Mikula, K., Preusser, T., Rumpf, M.: Morphological image sequence processing, *Computing and Visualization in Science*, Vol. 6, No. 4 (2004), 197–209

[14] Mikula, K., Sarti, A., Sgallari, F.: Co-Volume Level Set Method in Subjective Surface Based Medical Image Segmentation, *Handbook of Biomedical Image Analysis, Springer US* (2005) 583–626

[15] Montagnat, J., Delingette, H.: 4D deformable models with temporal constraints: application to 4D cardiac image segmentation, *in Medical Image Analysis (MedIA)*, 9 (1), (2005), 87–100

[16] Paragios, N.: Variational Methods and Partial Differential Equations in Cardiac Image Analysis, *Invited Publication : IEEE International Symposium on Biomedical Imaging: From Nano to Macro*, (2004)

[17] Perona, P., Malk, J.: Scale space and edge detection using anisotropic diffusion, *Proc. IEEE Computer Society Workshop on Computer Vision* (1987)

[18] Rousson, M., Paragios, N.: Prior Knowledge, Level Set Representations & Visual Grouping, *International Journal of Computer Vision Vol. 76, No. 3* (2008), 231–243,

[19] Sethian, J. A.: Level Set Methods, Cambridge University Press (1996)

[20] Zhao, H. K.: Fast sweeping method for eikonal equation, *Mathematics of Computation,* **74** (2005), 603–627

[1] IKEM Praha, `http://www.ikem.cz`

Radek Máca and Michal Beneš
Department of Mathematics, Faculty of Nuclear Sciences and Physical Engineering, Czech Technical University in Prague, Trojanova 13, 120 00, Praha 2, Czech Republic
E-mail: radek.maca(at)fjfi.cvut.cz
michal.benes(at)fjfi.cvut.cz

Jaroslav Tintěra
Department of Clinical and Experimental Spectroscopy, Institute for Clinical and Experimental Medicine, Vídeňská 1958/9 140 21, Praha 4, Czech Republic
E-mail: jati(at)ikem.cz